

# Introducing a Symmetry-Breaking Coupler into a Dielectric Metasurface Enables Robust High-Q Quasi-BICs

Gianni Q. Moretti, Andreas Tittl, Emiliano Cortés, Stefan A. Maier, Andrea V. Bragas, and Gustavo Grinblat\*

Dielectric metasurfaces supporting quasibound states in the continuum (quasi-BICs) exhibit very high-quality factor resonances and electric field confinement. However, accessing the high-Q end of the quasi-BIC regime usually requires marginally distorting the metasurface design from a BIC condition, pushing the needed nanoscale fabrication precision to the limit. This work introduces a novel concept for generating high-Q quasi-BICs, which strongly relaxes this requirement by incorporating a relatively large perturbative element close to high-symmetry points of an undistorted BIC metasurface, acting as a coupler to the radiation continuum. This approach is validated by adding a  $\approx 100$  nm diameter cylinder between two reflection-symmetry points separated by a 300 nm gap in an elliptical disk metasurface unit cell, using gallium phosphide as the dielectric. It is found that high-Q resonances emerge when the cylindrical coupler is placed at any position between such symmetry points. This metasurface's second harmonic generation capability in the optical range is further explored. Displacing the coupler as much as a full diameter from a BIC condition produces record-breaking normalized conversion efficiencies  $> 10^2 \text{ W}^{-1}$ . The strategy of enclosing a disruptive element between multiple high-symmetry points in a BIC metasurface can be applied to construct robust high-Q quasi-BICs in many geometrical designs.

among others. Recently, resonances originating from the concept of bound states in the continuum (BICs) have been shown to produce quality factors and field enhancements far higher than those of widely studied radiative Mie modes and nonradiative anapole states.<sup>[12–14]</sup> BICs are perfectly confined states which possess an infinite lifetime and therefore cannot couple to radiation channels.<sup>[15]</sup> Symmetry-protected BICs, the most studied type of BIC,<sup>[16]</sup> can be realized by introducing a symmetry-breaking perturbation, which typically involves slightly distorting the metasurface geometrical design, turning the optically inaccessible BIC into a high-quality factor quasi-BIC. Some examples in the literature include unit cells of pairs of slightly differently sized rods<sup>[17,18]</sup> or cylinders,<sup>[19,20]</sup> blocks,<sup>[21]</sup> and rings<sup>[22]</sup> with missing sections, as well as tilted elliptical cylinders.<sup>[23,24]</sup> The magnitude of the asymmetry in relation to the characteristic dimensions of the system can often be quantified by a dimensionless parameter  $\alpha$ ; for sufficiently small

perturbations, a proportionality relationship between the quality factor ( $Q$ , defined as the resonance frequency divided by its linewidth) and  $\alpha^{-2}$  can be obtained for most metasurface designs.<sup>[25]</sup>

Given the excellent field confinement abilities of quasi-BICs and the large intrinsic nonlinearities of high-index dielectrics, these platforms are especially useful to enhance nonlinear processes at subwavelength volumes. Over the last decade, second

## 1. Introduction


Dielectric metasurfaces can greatly enhance incident electromagnetic fields over a large area with very low absorption in the visible and infrared regions of the spectrum. They can controllably tailor the amplitude and phase of the light wave front,<sup>[1–4]</sup> efficiently generate nonlinear light,<sup>[5,6]</sup> and can be exploited for biosensing<sup>[7–9]</sup> and metrology applications,<sup>[10,11]</sup>

G. Q. Moretti, A. V. Bragas, G. Grinblat  
Departamento de Física, FCEN, IFIBA-CONICET  
Universidad de Buenos Aires  
Buenos Aires C1428EGA, Argentina  
E-mail: grinblat@df.uba.ar

A. Tittl, E. Cortés, S. A. Maier  
Chair in Hybrid Nanosystems  
Nanoinstitut Munich  
Faculty of Physics  
Ludwig-Maximilians-Universität München  
80539 München, Germany

S. A. Maier  
School of Physics and Astronomy  
Monash University  
Clayton, VIC 3800, Australia

S. A. Maier  
Department of Physics  
Imperial College London  
London SW7 2AZ, UK

 The ORCID identification number(s) for the author(s) of this article can be found under <https://doi.org/10.1002/adpr.202200111>.

© 2022 The Authors. Advanced Photonics Research published by Wiley-VCH GmbH. This is an open access article under the terms of the Creative Commons Attribution License, which permits use, distribution and reproduction in any medium, provided the original work is properly cited.

DOI: 10.1002/adpr.202200111

and third harmonic generation (SHG and THG, respectively) have been extensively studied using metallic and dielectric nanostructures,<sup>[26–30]</sup> with research only recently focusing on quasi-BIC resonances.<sup>[17,24,31–34]</sup> Obtained experimental conversion efficiencies ( $\eta_{\text{SHG}} = P_{2\omega}/P_{\omega}$  and  $\eta_{\text{THG}} = P_{3\omega}/P_{\omega}$ ) reached  $\approx 0.01\%$ ,<sup>[32,35,36]</sup> while normalized efficiencies ( $\xi_{\text{SHG}} = \eta_{\text{SHG}}/P_{\omega}$  and  $\xi_{\text{THG}} = \eta_{\text{THG}}/P_{\omega}^2$ ) up to  $0.04 \text{ W}^{-1} (\text{SHG})$ <sup>[24]</sup> and  $1 \times 10^{-5} \text{ W}^{-2}$  (THG)<sup>[21]</sup> were achieved. On the other hand, several theoretical works have predicted significantly better performances.<sup>[6,18,37,38]</sup> However, as they have considered the perturbative nonlinear regime, their validity only holds for sufficiently small incident intensities at relatively low field amplifications. Because of the strong near-field enhancements present in quasi-BICs, pump depletion and the optical Kerr effect become important. This issue has been recently addressed for SHG, demonstrating a maximum theoretical conversion efficiency of  $0.2\%$  at  $100 \text{ kW cm}^{-2}$  in an AlGaAs metasurface.<sup>[39]</sup> However, an unrealistic asymmetry parameter as small as  $\alpha < 0.02$  was assumed, well below the current experimental limit of  $\alpha = 0.1$  for the same system design.<sup>[24]</sup>

In this work, we propose a different method to break symmetries in BIC-based metasurfaces. Instead of slightly modifying the geometry of the meta-atoms, we add a perturbative element to the unaltered BIC metasurface to enable coupling to radiation channels. By placing such an element close to a relevant high-symmetry point of the array, the resulting metasurface supports very high-Q resonances. As a unit cell can hold more than one such symmetry point, the dependence of the quality factor on the introduced asymmetry is, in general, no longer monotonous. We focus on the extensively studied BIC metasurface design defined by a unit cell of two elliptical cylinders.<sup>[7,8,13,24]</sup> To generate the quasi-BIC, the reflection symmetry of this system is usually broken by slightly tilting the elliptical disks toward each other. Here, we show that a resonance of the same nature is more efficiently excited by adding an off-center cylindrical coupler while keeping the elliptical disks parallel (see schematic in **Figure 1**). We choose gallium phosphide (GaP) as the high-index dielectric ( $n > 3$ ), as it possesses negligible absorption in the majority of the visible spectrum and large nonlinearities.<sup>[40–42]</sup> We model the SHG capabilities of our design in the nonperturbative regime and demonstrate conversion efficiencies up to  $0.5\%$  at pump intensities  $< 1 \text{ kW cm}^{-2}$ .

## 2. Results

The geometries of the studied GaP metasurfaces are depicted in **Figure 2A**. The short ( $D_1$ ) and long diameters ( $D_2$ ) of the elliptical cylinders are 170 and 380 nm, respectively, the height is 200 nm, the center-to-center distance between adjacent meta-atoms ( $d$ ) is 300 nm, and the square lattice period ( $p$ ) is 600 nm. These sizes were chosen to obtain a quasi-BIC resonance at a wavelength of  $\approx 970 \text{ nm}$ , following our previous work,<sup>[14]</sup> so that the second harmonic wavelength falls in the transparency range of GaP ( $\lambda > 450 \text{ nm}$ ), and the second-order susceptibility is maximum. For the conventional metasurface configuration (left panel), used as a reference, the asymmetry parameter is defined as  $\alpha_1 = \sin(\theta)$ , with  $\theta$  the tilt angle. In the proposed design (right panel),  $\theta$  is kept fixed at  $\theta = 0$ , and a cylinder of diameter  $D$  is

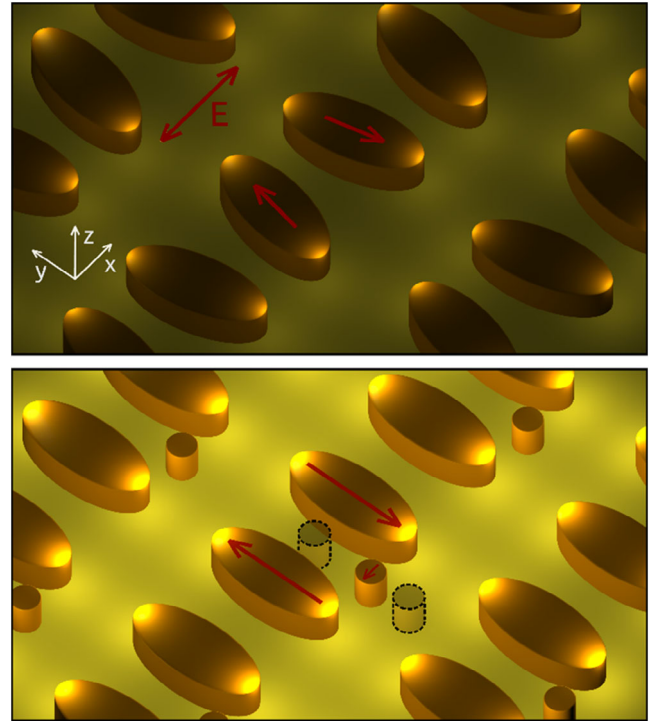


**Figure 1.** Elliptical cylinder metasurfaces with introduced reflection asymmetries in the  $y$ -direction. For the configuration on the top, an  $x$ -polarized electric field excites a quasi-BIC resonance, as enabled by the inward tilting of the meta-atoms. A more intense quasi-BIC (bottom) of the same character can be excited by adding an off-center cylindrical coupler between reflection-symmetry positions, marked with semitransparent cylinders in a representative unit cell.

added between two reflection-symmetry points (marked as crosses) separated by  $w = 300 \text{ nm}$ , acting as a coupler to radiation channels. In this case, the asymmetry parameter is defined as  $\alpha_2 = \Delta y/w$ , where  $\Delta y$  is the displaced distance of the cylindrical coupler in the  $y$ -direction from the bottom reflection-symmetry point. Note that the vertical reflection symmetry is broken in both metasurfaces, while the horizontal reflection symmetry is maintained.

To compare the optical resonances of the two configurations, we initially set the coupler diameter to  $D = 80 \text{ nm}$  and compute the transmission ( $T$ ) and the average intensity enhancement inside the dielectric ( $\langle |E/E_0|^2 \rangle$ ) as a function of the incident wavelength for  $\alpha$  approaching 0 (see Methods for specifics on numerical simulations). The tilt angle is varied from  $10$  to  $1^\circ$  ( $\alpha_1$  ranging from  $\approx 0.2$  to  $\approx 0.02$ ) and  $\Delta y$  from  $150$  to  $10 \text{ nm}$  ( $\alpha_2$  from  $0.5$  to  $\approx 0.03$ ), respectively. As can be seen in **Figure 2B**, the quality factor and the field enhancement diverge when  $\theta \rightarrow 0$  and  $\Delta y \rightarrow 0$ , while the resonance position converges to (approximately) the same BIC wavelength from opposite sides of the spectrum. However, significantly larger field enhancements are found for the three-element unit cell design. To better illustrate the advantage of this geometry, **Figure 2C** compares the electric field distribution for both metasurfaces at  $\alpha_{1,2} = 0.2$  (corresponding to  $\theta = 12^\circ$  and  $\Delta y = 60 \text{ nm}$ , respectively). We observe that the proposed design provides a 30-fold increase in field amplification

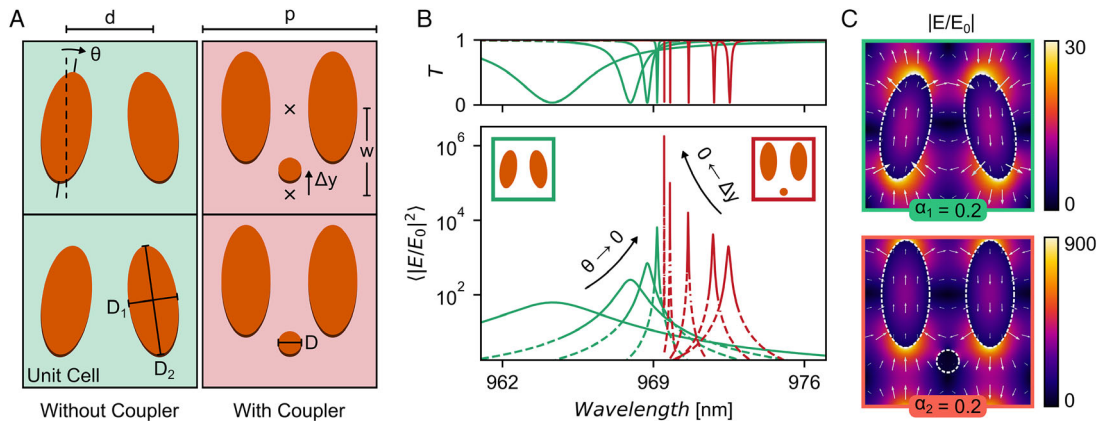


**Figure 2.** Field enhancement performance of quasi-BIC metasurfaces. A) Schematics of the analyzed metasurfaces, showing two adjacent unit cells for each of them. On the left, the asymmetry is introduced by tilting the meta-atoms inward. On the right, a cylindrical coupler is added between two reflection-symmetry points. B) Computed transmission ( $T$ ) of the metasurfaces (top) and average intensity enhancement inside the dielectric (bottom) as a function of incident wavelength. Different  $\theta$  and  $\Delta y$  values are compared to illustrate the behavior when approaching zero asymmetry. C) Electric field distribution (magnitude and direction) in the  $xy$  plane when considering the same asymmetry parameter value for both metasurfaces.

compared to the reference case, which corresponds to an increase of the intensity enhancement by a factor of  $\approx 1000$ . In both metasurfaces, the excited mode consists of in-plane electric quadrupole and out-of-plane magnetic dipole components, which couple to the external  $x$ -polarized incident radiation through an electric dipole in the  $x$ -direction, as enabled by the introduced asymmetries<sup>[13,43]</sup> (details of the multipolar decompositions can be found in Figure S1, Supporting Information). Note that making  $\Delta x \neq 0$  (i.e., displacing the coupler in the  $x$ -direction) at  $\Delta y \neq 0$  would introduce additional asymmetry, decreasing the quality factor of the resonance, as shown in Figure 3A for  $\Delta y = 40$  nm. On the other hand, taking  $\Delta x \neq 0$  at  $\Delta y = 0$  would produce no quasi-BIC resonance because it would unbalance the compensated electric field of the BIC in the  $y$ -direction only, preventing any coupling with the incoming  $x$ -polarized beam, as can be deduced from the ideal BIC field distribution in Figure 3B. Breaking the symmetry solely via  $\Delta y \neq 0$  as in Figure 2 corresponds to moving the coupler along a  $E_y = 0$  line (see Figure 3B, right panel), enabling fine control of the electric polarization in the  $x$ -direction, with no further distortion of the BIC condition.

To evaluate the influence of the coupler diameter on the resonant properties, in Figure 4A we present the dependence of  $Q$  on  $D$  as a function of  $\alpha_2$  at  $\Delta x = 0$ . We find a proportionality relationship between  $Q$  and  $\alpha_2^{-2}$  that holds for all explored diameters at sufficiently small displacement asymmetries, analogous to  $Q$  versus  $\alpha_1^{-2}$  for the reference metasurface (shown as a solid line). In the tilted design, introducing small  $\theta$  angles linearly changes the net magnitude of  $E_x$ ,<sup>[25]</sup> in a similar way to moving the coupler away from  $\Delta y = 0$ , as can be inferred from Figure 3C, explaining the common trend. In Figure 4A, we also find that enlarging the size of the coupler at same  $\alpha_2$  decreases the quality factor of the resonance, acting as an alternate way of increasing the degree of symmetry perturbation. Nevertheless, even for disk diameters as large as 160 nm, this system performs significantly better than the reference metasurface. This can be

understood by noting that tilting the elliptical disks can be thought of as displacing four bulky couplers (the four tips of the two meta-atoms) from the BIC condition, corresponding to a much larger symmetry distortion.

As can be seen in Figure 2 and 3, the proposed metasurface presents two high-symmetry points with  $E_x = 0$  and  $E_y = 0$ , corresponding to  $\Delta y = 0$  and  $\Delta y = 300$  nm, connected by a  $E_y = 0$  line. Hence, when continuously varying  $\Delta y$ , a second BIC condition should be found. This becomes evident when plotting the dependence of  $Q$  on  $\Delta y$  for the whole displacement range, as shown in Figure 4B for two disk diameters,  $D = 60$  nm and  $D = 80$  nm, which are sizes that can fit comfortably within the 130 nm gap between adjacent elliptical cylinders. In contrast to the reference metasurface, the quality factor never approaches zero, staying always above  $10^3$  and  $10^4$  for  $D = 80$  nm and  $D = 60$  nm, respectively, as the coupler is “trapped” between two BIC conditions. As shown in Figure 4C, the nature of the excited quasi-BIC remains the same when approaching both high-symmetry points, with reduced field enhancement near the high end of the  $\Delta y$  range. As the magnitude of the BIC  $E_x$ -field increases with steeper slope close to  $\Delta y = 300$  nm as compared to  $\Delta y = 0$  (Figure 3C), placing the coupler near  $\Delta y = 300$  nm generates stronger field perturbations and hence weaker quasi-BICs. These findings offer great advantages for the realization of BIC-based metasurfaces with high robustness against fabrication inaccuracies, as even experimentally straightforward displacement distances of 100 nm can produce quality factors as high as  $10^5$ . In comparison, the reference design would require an unfeasible tilt angle of  $< 0.5^\circ$ , which corresponds to moving the tips of the meta-atoms from their straight positions by just  $\approx 1$  nm. While the coupler can be conveniently chosen to be of any size and placed at positions weakly perturbing the BIC field distribution, the conventional strategy of tilting the meta-atoms displaces large pieces of material of fixed size around their immediate surrounding, strongly disturbing high-field regions.

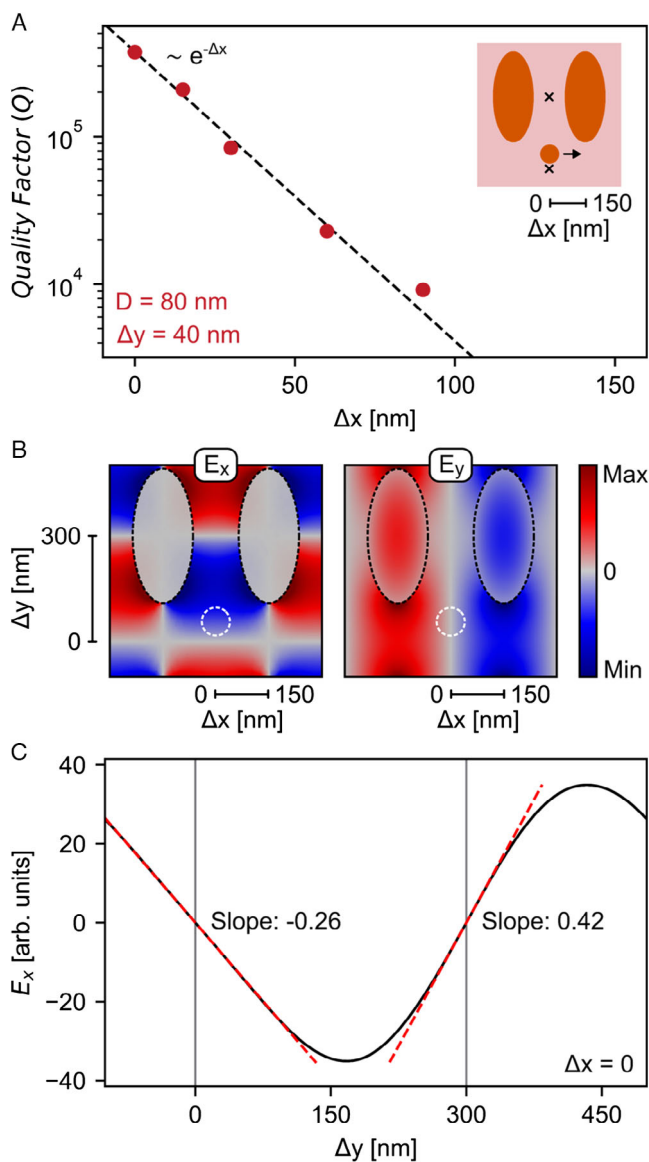


**Figure 3.** Breaking the reflection symmetry in the  $x$ - and  $y$ -directions. A) Quality factor of the resonance when displacing the cylindrical coupler along the  $x$ -direction at  $\Delta y = 40$  nm. A nearly exponential decay is observed when increasing  $\Delta x$ . B) In-plane electric field distribution of the ideal BIC condition (parallel elliptical cylinders with no coupler element). The eigenstate has fully compensated in-plane electric fields, with no possible coupling to linearly polarized light. Adding a coupler to this configuration (as represented in white) would unbalance the BIC field distribution depending on its position. C) Dependence of  $E_x$  on  $\Delta y$  at  $\Delta x = 0$ , as extracted from panel B. Positioning the coupler close to  $\Delta y = 0$  would produce a greater unbalance of the field, as compared to  $\Delta y = 300$  nm, for same relative displacement.

The enhanced electric field inside the metasurface makes it attractive for studying nonlinear processes arising from the intrinsic nonlinear properties of GaP. In **Figure 5**, we analyze the SHG performance of our metasurface, considering a diameter of 80 nm for the cylindrical coupler (see Experimental Section for nonlinear simulation details). First, we study how the

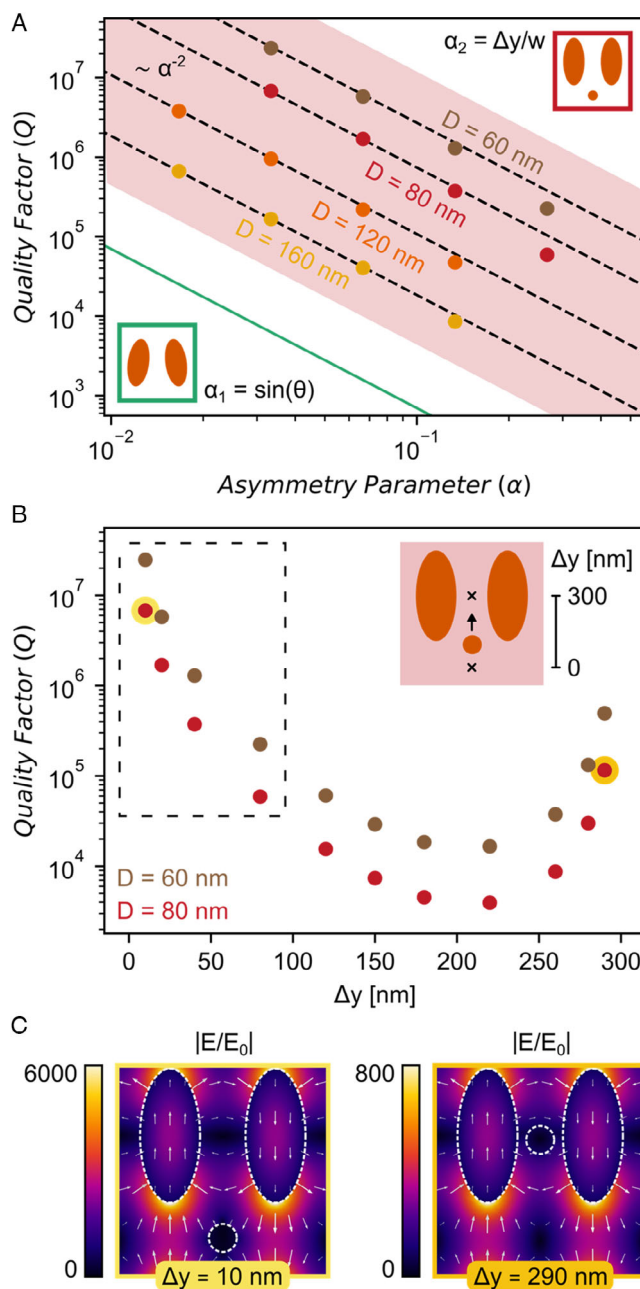


**Figure 4.** Detailed analysis of the quasi-BIC resonances. A) Quality factor of the resonance as a function of the asymmetry parameter for both configurations, considering different coupler diameters. The dotted and solid lines follow a linear relationship between  $Q$  and  $\alpha^{-2}$ . Maximum  $\alpha_2$  in the plot corresponds to  $\Delta y = 80$  nm. B) Quality factor for  $\Delta y$  values up to 290 nm, for two particular coupler diameters. The dashed region corresponds to the asymmetries displayed in (A). C) Electric field distribution close to the two BIC conditions for  $D = 80$  nm.

nonlinear response varies when modifying the in-plane orientation of GaP crystal lattice. The [100] crystal direction is set initially along the  $x$ -direction of the coordinate system. As seen in **Figure 5A**, a rotation in the crystal plane of  $\beta = 45^\circ$  gives the maximum enhancement of efficiency. This corresponds to the [110]

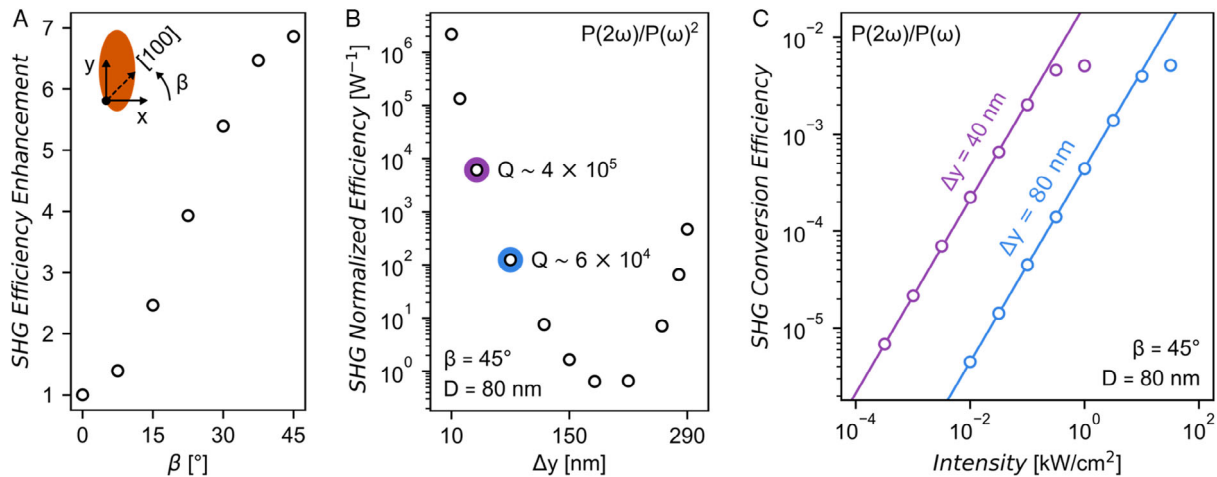


**Figure 5.** Second harmonic efficiency calculations. A) SHG efficiency enhancement when varying the in-plane crystal orientation angle  $\beta$ . B) Normalized conversion efficiency at  $\beta = 45^\circ$  as a function of  $\Delta y$  for  $D = 80$  nm, computed in the perturbative regime. C) Dependence of the SHG conversion efficiency on the pump intensity for the two cases highlighted in (B), considering pump depletion and the optical Kerr effect. The computed data (shown as circles) deviate from the perturbative behavior (solid lines) at approximately 0.1 and 10  $\text{kW cm}^{-2}$ , respectively.

crystal direction becoming aligned with the fundamental electric field inside the material, which accommodates mainly along the  $y$ -direction (see Figure 2C and 4C). The nonlinear polarization is most efficiently excited in this condition given the symmetry of GaP nonlinear susceptibility tensor.<sup>[44]</sup>

In Figure 5B, the normalized SHG efficiency in the perturbative regime is calculated as a function of  $\Delta y$  in the 10–290 nm range at  $\beta = 45^\circ$ , revealing values between  $\sim 1$  and  $10^6 \text{ W}^{-1}$ . In particular, for metasurfaces with quality factors around  $10^5$  ( $\Delta y = 40\text{--}80$  nm), above which nonradiative contributions due to sample imperfections—not considered in our model—become important,<sup>[21]</sup> the normalized efficiency reaches the order of  $10^3 \text{ W}^{-1}$ . This performance exceeds the highest previously reported theoretical values by three orders of magnitude.<sup>[14]</sup> We then study the nonperturbative regime, considering pump depletion and the optical Kerr effect, which are no longer negligible even for relatively low pump intensities. In this regime, the resulting large second harmonic field interacts with and depletes the fundamental field, while the ultrahigh field enhancement distorts the resonant condition through the intensity-dependent refractive index (to expand on this refer to Figure S4, Supporting Information). Consequently, we find that the conversion efficiency saturates around 0.5%, as can be seen in Figure 5C. We also observe that the saturation power decreases when increasing the field confinement ability of the resonator (i.e., for smaller asymmetries), as expected. Remarkably, for the metasurface with  $\Delta y = 40$  nm, the saturation regime would be reached with pump powers as low as 1 mW, when considering an excitation area of hundreds of  $\mu\text{m}^2$  covering thousands of unit cells. These conditions could be achieved with a simple low-cost continuous-wave laser pointer and a common low numerical aperture lens. We note that the damage threshold of GaP in its transparency range is about  $0.7 \text{ GW cm}^{-2}$ ,<sup>[45]</sup> which is well above the effective pump intensity of  $<0.1 \text{ GW cm}^{-2}$  that we compute by considering the field enhancement within the dielectric material.

### 3. Conclusion

In summary, we demonstrate a novel strategy to generate robust high-Q quasi-BICs in dielectric metasurfaces. By introducing a symmetry-breaking element into a BIC-supporting unit cell, the coupling to the radiation continuum can be controlled with much better precision than through the usual distorting of the actual metasurface. We test this approach by adding a small cylinder (60–160 nm diameter) to an array of parallel elliptical cylinder GaP meta-atoms. By enclosing the cylindrical coupler between two BIC reflection-symmetry points, high-Q resonances emerge along the whole 300 nm long region between the BIC conditions. We then optimize the SHG capabilities of this system by choosing the more convenient in-plane GaP crystal orientation and perform perturbative and nonperturbative nonlinear studies, considering pump depletion and the optical Kerr effect. In the perturbative regime, the conversion efficiency grows linearly with the intensity enhancement of the resonance, while a maximum conversion efficiency of 0.5% is obtained in the nonperturbative approach, at only  $<1 \text{ kW cm}^{-2}$  pump intensity. The ultrastrong nonlinear response of this metasurface makes it a very suitable candidate for various nonlinear nanophotonic applications. Furthermore, the robustness of the proposed method for breaking symmetries in BIC metasurfaces can also benefit many other unit cell configurations and improve the performance of a broad range of practical applications from ultrasensitive biodetection to surface-enhanced energy conversion processes.

### 4. Experimental Section

The linear and nonlinear numerical calculations were performed using the RF module of the COMSOL Multiphysics software.<sup>[46]</sup> The GaP structures composing the unit cell were placed on a glass/air interface in a square prism domain geometry with periodic boundary conditions in the four lateral faces and a perfectly-matched layer (PML) in the top and bottom faces.

The linear optical studies were carried out by solving the problem for the scattered field, using the analytical expressions of the reflection and transmission Fresnel coefficients at the air/glass interface to define the background field. The complex permittivity of GaP used for the simulations was taken from the literature.<sup>[40]</sup> Values of  $\epsilon = 2.25$  and  $\epsilon = 1$  for the glass and air domains were utilized, respectively.

The nonlinear calculations were performed with an iterative, segregated approach. For the perturbative simulation, the resulting linearly excited fields within the nanostructures were used to compute a second-order polarization with frequency  $2\omega$  in the material, and then used as a source to obtain the nonlinear fields. In the nonperturbative condition (pump depletion and optical Kerr effect added to the linear polarization), the second harmonic solution was used again in the linear computation, leading to a different nonlinear field. This was iteratively done until convergence was achieved.

The second-order susceptibility tensor used to compute the nonlinear polarization was taken from the literature.<sup>[41,42]</sup> GaP has a zinc-blende crystal structure with a nonlinear tensor of the form  $\chi^{(2)}_{ijk} \neq 0$  for  $i \neq j \neq k$ , with all six nonzero components having the same value of  $2 \times 10^{-10} \text{ m V}^{-1}$  at a wavelength of 970 nm. For the optical Kerr effect, we computed a third-order susceptibility of  $4.3 \times 10^{-19} \text{ m}^2 \text{ V}^{-2}$ , derived from the experimentally reported magnitude of the nonlinear index  $n_2 = 10^{-17} \text{ m}^2 \text{ W}^{-1}$ .<sup>[42]</sup> With these considerations, the added polarizations to the field equations at  $\omega$  and  $2\omega$  are

$$P_i(\omega) = \epsilon_0 \chi^{(2)} E_{2j} E_{1k}^* + \epsilon_0 \chi^{(3)} (|E_1|^2 E_i + 2E_{1i} (E_{1j} E_{1j}^* + E_{1k} E_{1k}^*)) \quad (1)$$

$$P_i(2\omega) = 2\epsilon_0 \chi^{(2)} E_{1j} E_{1k} \quad (2)$$

where, in all cases,  $i \neq j \neq k$ ,  $E_1 = E(\omega)$ , and  $E_2 = E(2\omega)$ .

The SHG conversion efficiency was computed as the ratio between the nonlinear Poynting vector integrated over the top and bottom limits of the simulation domain and the incident power over the surface area of a unit cell ( $600 \times 600 \text{ nm}^2$ ).

The multipolar decompositions shown in the Supporting Information were calculated using Cartesian decomposition.<sup>[47]</sup>

## Supporting Information

Supporting Information is available from the Wiley Online Library or from the author.

## Acknowledgements

This work was partially supported by PICT 2017-2534, PICT 2019-01886, PIP 112 201301 00619, PIP 112 202001 01465, UBACyT Proyecto 20020170100432BA, and UBACyT Proyecto 20020190200296BA. The authors also acknowledge funding and support from the Deutsche Forschungsgemeinschaft (DFG, German Research Foundation) under grant numbers EXC 2089/1-390776260 (Germany's Excellence Strategy) and TI 1063/1 (Emmy Noether Program), the Bavarian program Solar Energies Go Hybrid (SolTech), the Center for NanoScience (CeNS), the DAAD Programme for Project-Related Personal Exchange (PPP) 57573042, the European Commission for the ERC-STG Catalight 802989, and the Lee-Lucas Chair in Physics. S.A.M. additionally acknowledges the EPSRC (EP/W017075/1).

## Conflict of Interest

The authors declare no conflict of interest.

## Data Availability Statement

The data that support the findings of this study are available from the corresponding author upon reasonable request.

## Keywords

bound states in the continuum, dielectric metasurfaces, nanophotonics, second-harmonic generation

Received: April 14, 2022

Revised: July 16, 2022

Published online:

- [1] G. Qu, W. Yang, Q. Song, Y. Liu, C.-W. Qiu, J. Han, D.-P. Tsai, S. Xiao, *Nat. Commun.* **2020**, *11*, 5484.
- [2] C. Zhang, S. Divitt, Q. Fan, W. Zhu, A. Agrawal, Y. Lu, T. Xu, H. J. Lezec, *Light Sci. Appl.* **2020**, *9*, 55.
- [3] W. T. Chen, A. Y. Zhu, V. Sanjeev, M. Khorasaninejad, Z. Shi, E. Lee, F. Capasso, *Nat. Nanotechnol.* **2018**, *13*, 220.
- [4] A. Arbabi, Y. Horie, M. Bagheri, A. Faraon, *Nat. Nanotechnol.* **2015**, *10*, 937.
- [5] H. Liu, C. Guo, G. Vampa, J. L. Zhang, T. Sarmiento, M. Xiao, P. H. Bucksbaum, J. Vučković, S. Fan, D. A. Reis, *Nat. Phys.* **2018**, *14*, 1006.
- [6] L. Kang, L. Kang, H. Bao, D. H. Werner, D. H. Werner, *Opt. Lett.* **2021**, *46*, 633.
- [7] F. Yesilkoy, E. R. Arvelo, Y. Jahani, M. Liu, A. Tittl, V. Cevher, Y. Kivshar, H. Altug, *Nat. Photonics* **2019**, *13*, 390.
- [8] A. Tittl, A. Leitis, M. Liu, F. Yesilkoy, D.-Y. Choi, D. N. Neshev, Y. S. Kivshar, H. Altug, *Science* **2018**, *360*, 1105.
- [9] B. Ma, A. Ouyang, J. Zhong, P. A. Belov, R. K. Sinha, W. Qian, P. Ghosh, Q. Li, *Electronics* **2021**, *10*, 1363.
- [10] C. Jin, M. Afsharnia, R. Berlich, S. Fasold, C. Zou, D. Arslan, I. Staude, T. Pertsch, F. Setzpfandt, *Adv. Photonics* **2019**, *1*, 036001.
- [11] G. H. Yuan, N. I. Zheludev, *Science* **2019**, *364*, 771.
- [12] V. R. Tuz, V. V. Khardikov, A. S. Kupriianov, K. L. Domina, S. Xu, H. Wang, H.-B. Sun, *Opt. Express* **2018**, *26*, 2905.
- [13] M. Liu, D.-Y. Choi, *Nano Lett.* **2018**, *18*, 8062.
- [14] G. Q. Moretti, E. Cortés, S. A. Maier, A. V. Bragas, G. Grinblat, *Nanophotonics* **2021**, *10*, 4261.
- [15] C. W. Hsu, B. Zhen, A. D. Stone, J. D. Joannopoulos, M. Soljačić, *Nat. Rev. Mater.* **2016**, *1*, 16048.
- [16] S. Joseph, S. Pandey, S. Sarkar, J. Joseph, *Nanophotonics* **2021**, *10*, 4175.
- [17] K. Koshelev, Y. Tang, K. Li, D.-Y. Choi, G. Li, Y. Kivshar, *ACS Photonics* **2019**, *6*, 1639.
- [18] M. Gandolfi, A. Tognazzi, D. Rocco, C. De Angelis, L. Carletti, *Phys. Rev. A* **2021**, *104*, 023524.
- [19] R. Masoudian Saadabad, L. Huang, A. E. Miroshnichenko, *Phys. Rev. B* **2021**, *104*, 235405.
- [20] P. Vaity, H. Gupta, A. Kala, S. Dutta Gupta, Y. S. Kivshar, V. R. Tuz, V. G. Achanta, *Adv. Photonics Res.* **2022**, *3*, 2100144.
- [21] Z. Liu, Y. Xu, Y. Lin, J. Xiang, T. Feng, Q. Cao, J. Li, S. Lan, J. Liu, *Phys. Rev. Lett.* **2019**, *123*, 253901.
- [22] C. Zhou, X. Qu, S. Xiao, M. Fan, *Phys. Rev. Appl.* **2020**, *14*, 044009.
- [23] J. Tian, Q. Li, P. A. Belov, R. K. Sinha, W. Qian, M. Qiu, *ACS Photonics* **2020**, *7*, 1436.
- [24] A. P. Anthur, H. Zhang, R. Paniagua-Dominguez, D. A. Kalashnikov, S. T. Ha, T. W. W. Maß, A. I. Kuznetsov, L. Krivitsky, *Nano Lett.* **2020**, *20*, 8745.

- [25] K. Koshelev, S. Lepeshov, M. Liu, A. Bogdanov, Y. Kivshar, *Phys. Rev. Lett.* **2018**, *121*, 193903.
- [26] K. Thyagarajan, J. Butet, O. J. F. Martin, *Nano Lett.* **2013**, *13*, 1847.
- [27] G. Grinblat, M. Rahmani, E. Cortés, M. Caldarola, D. Comedi, S. A. Maier, A. V. Bragas, *Nano Lett.* **2014**, *14*, 6660.
- [28] J. Cambiasso, G. Grinblat, Y. Li, A. Rakovich, E. Cortés, S. A. Maier, *Nano Lett.* **2017**, *17*, 1219.
- [29] G. Grinblat, Y. Li, M. P. Nielsen, R. F. Oulton, S. A. Maier, *Nano Lett.* **2016**, *16*, 4635.
- [30] M. R. Shcherbakov, D. N. Neshev, B. Hopkins, A. S. Shorokhov, I. Staude, E. V. Melik-Gaykazyan, M. Decker, A. A. Ezhov, A. E. Miroshnichenko, I. Brener, A. A. Fedyanin, Y. S. Kivshar, *Nano Lett.* **2014**, *14*, 6488.
- [31] P. P. Vabishchevich, S. Liu, M. B. Sinclair, G. A. Keeler, G. M. Peake, I. Brener, *ACS Photonics* **2018**, *5*, 1685.
- [32] K. Koshelev, S. Kruk, E. Melik-Gaykazyan, J.-H. Choi, A. Bogdanov, H.-G. Park, Y. Kivshar, *Science* **2020**, *367*, 288.
- [33] G. Grinblat, *ACS Photonics* **2021**, *8*, 3406.
- [34] G. Zograf, K. Koshelev, A. Zalogina, V. Korolev, R. Hollinger, D.-Y. Choi, M. Zuerch, C. Spielmann, B. Luther-Davies, D. Kartashov, S. V. Makarov, S. S. Kruk, Y. Kivshar, *ACS Photonics* **2022**, *9*, 567.
- [35] R. Camacho-Morales, M. Rahmani, S. Kruk, L. Wang, L. Xu, D. A. Smirnova, A. S. Solntsev, A. Miroshnichenko, H. H. Tan, F. Karouta, S. Naureen, K. Vora, L. Carletti, C. De Angelis, C. Jagadish, Y. S. Kivshar, D. N. Neshev, *Nano Lett.* **2016**, *16*, 7191.
- [36] G. Grinblat, Y. Li, M. P. Nielsen, R. F. Oulton, S. A. Maier, *ACS Nano* **2017**, *11*, 953.
- [37] L. Carletti, K. Koshelev, C. De Angelis, Y. Kivshar, *Phys. Rev. Lett.* **2018**, *121*, 033903.
- [38] Z. Han, F. Ding, Y. Cai, U. Levy, *Nanophotonics* **2021**, *10*, 1189.
- [39] T. Ning, T. Ning, X. Li, X. Li, Z. Zhang, Z. Zhang, Y. Huo, Y. Huo, Q. Yue, Q. Yue, L. Zhao, L. Zhao, Y. Gao, Y. Gao, *Opt. Express* **2021**, *29*, 17286.
- [40] S. Adachi, *J. Appl. Phys.* **1989**, *66*, 6030.
- [41] I. Shoji, T. Kondo, A. Kitamoto, M. Shirane, R. Ito, *J. Opt. Soc. Am. B* **1997**, *14*, 2268.
- [42] D. J. Wilson, K. Schneider, S. Hönl, M. Anderson, Y. Baumgartner, L. Czornomaz, T. J. Kippenberg, P. Seidler, *Nat. Photonics* **2020**, *14*, 57.
- [43] M. Liu, D. A. Powell, R. Guo, I. V. Shadrivov, Y. S. Kivshar, *Advanced Optical Materials* **2017**, *5*, 1600760.
- [44] R. W. Boyd, *Nonlinear Optics*, Academic Press, Amsterdam, **2008**, Ch 1.5.
- [45] L. P. Gonzalez, S. Guha, S. B. Trivedi, In CLEO, San Francisco, CA, **2004**.
- [46] COMSOL Multiphysics v. 5.4 www.comsol.com COMSOL AB, Stockholm.
- [47] E. A. Gurvitz, K. S. Ladutenko, P. A. Dergachev, A. B. Evlyukhin, A. E. Miroshnichenko, A. S. Shalin, *Laser Photonics Rev.* **2019**, *13*, 1800266.